

# OpenGeMM: A High-Utilization GeMM Accelerator Generator with Lightweight RISC-V Control and Tight Memory Coupling

Xiaoling Yi<sup>1</sup>, Ryan Antonio<sup>1</sup>, Joren Dumoulin<sup>1</sup>, Jiacong Sun<sup>1</sup>, Josse Van Delm<sup>1</sup>, Guilherme Paim<sup>1,2</sup>,

Marian Verhelst<sup>1</sup>

<sup>1</sup>MICAS-ESAT, KU Leuven

Leuven, Belgium

<sup>2</sup>INESC-ID, Instituto Superior Técnico, Universidade de Lisboa

Lisbon, Portugal

## ABSTRACT

Deep neural networks (DNNs) face significant challenges when deployed on resource-constrained extreme edge devices due to their computational and data-intensive nature. While standalone accelerators tailored for specific application scenarios suffer from inflexible control and limited programmability, generic hardware acceleration platforms coupled with RISC-V CPUs can enable high reusability and flexibility, yet typically at the expense of system-level efficiency and low utilization.

To fill this gap, we propose *OpenGeMM*, an open-source acceleration platform, jointly demonstrating high efficiency and utilization, as well as ease of configurability and programmability. *OpenGeMM* encompasses a parameterized Chisel-coded GeMM accelerator, a lightweight RISC-V processor, and a tightly coupled multi-banked scratchpad memory. The GeMM core utilization and system efficiency are boosted through three mechanisms: configuration pre-loading, input pre-fetching with output buffering, and programmable strided memory access. Experimental results show that *OpenGeMM* can consistently achieve hardware utilization ranging from 81.89% to 99.34% across diverse CNN and Transformer workloads. Compared to the SotA open-source Gemmini accelerator, *OpenGeMM* demonstrates a 3.58× to 16.40× speedup on normalized throughput across a wide variety of GeMM workloads, while achieving 4.68 TOPS/W system efficiency.

## KEYWORDS

Matrix Multiplication, GeMM Accelerator, Hardware Generators, RISC-V, Tight Memory Coupling, Open Source.

### ACM Reference Format:

Xiaoling Yi<sup>1</sup>, Ryan Antonio<sup>1</sup>, Joren Dumoulin<sup>1</sup>, Jiacong Sun<sup>1</sup>, Josse Van Delm<sup>1</sup>, Guilherme Paim<sup>1,2</sup>, Marian Verhelst<sup>1</sup>. 2025. OpenGeMM: A High-Utilization GeMM Accelerator Generator with Lightweight RISC-V Control and Tight Memory Coupling. In *30th Asia and South Pacific Design Automation Conference (ASPDAC '25)*, January 20–23, 2025, Tokyo, Japan. ACM, New York, NY, USA, 7 pages. <https://doi.org/10.1145/3658617.3697652>

Permission to make digital or hard copies of all or part of this work for personal or classroom use is granted without fee provided that copies are not made or distributed for profit or commercial advantage and that copies bear this notice and the full citation on the first page. Copyrights for components of this work owned by others than the author(s) must be honored. Abstracting with credit is permitted. To copy otherwise, or republish, to post on servers or to redistribute to lists, requires prior specific permission and/or a fee. Request permissions from [permissions@acm.org](mailto:permissions@acm.org).  
ASPDAC '25, January 20–23, 2025, Tokyo, Japan

© 2025 Copyright held by the owner/author(s). Publication rights licensed to ACM.  
ACM ISBN 979-8-4007-0635-6/25/01  
<https://doi.org/10.1145/3658617.3697652>

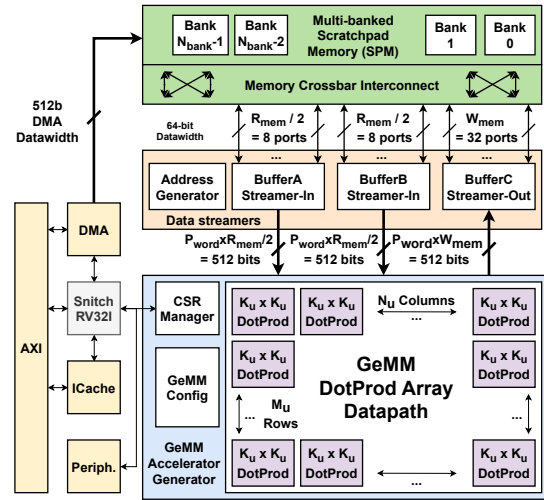


Figure 1: *OpenGeMM* platform overview.

## 1 INTRODUCTION

DNN models have been rapidly integrated into various aspects of our society, bringing a blossom of novel applications. However, they also bring a voracious demand for ever more computing power, presenting significant challenges for efficient execution. This problem is particularly severe when deploying DNNs at the edge, such as in-vehicle and wearable devices, where stringent power and area constraints exist [1].

A variety of domain-specific DNN accelerators have emerged in recent years, with remarkable performance and energy efficiency [2, 3]. However, these accelerators are typically tailored to specific workloads [4–6], hindering their reusability across diverse applications. Furthermore, they are often equipped with dedicated control and data interfaces, posing substantial challenges to smoothly integrating them into standard SoCs. For instance, deploying the NVDLA accelerator [7] requires additional wrappers and a custom compiler for signal translation when communicating to a host system [8, 9].

Alternatively, hardware acceleration platforms are proposed that include flexible DNN accelerators capable of targeting general computation kernels like general matrix multiplication (GeMM). These platforms integrate with a RISC-V host CPU, aiming to enhance hardware programmability and reusability [10–15]. While this solution appears promising, existing platforms face two important challenges: 1.) It is difficult to keep the control overhead negligible,

in order to not undermine the efficiency benefits of the accelerators. For example, the well-known Gemmini platform [12] employs a hardware generator design methodology and standard RISC-V control interface [16], facilitating rapid design-time flexibility and seamless system integration. However, it introduces significant control overhead with a bulky host CPU, i.e. a 5-stage pipeline in-order 64-bit Rocket control core. The CPU host occupies  $1.47\times$  more area than the spatial GeMM array [12]. 2.) It is hard to maintain a high utilization across diverse workloads, causing significant penalties on the system performance. Acceleration platforms must be carefully designed to minimize spatial and temporal underutilization of the DNN accelerators since each model/layer has different computation characteristics [13, 17, 18]. Low spatial utilization arises from inefficient exploitation of the available parallelism while low temporal utilization stems from idle cycles caused by long configuration times or memory stalls [19].

To overcome the challenges towards a highly efficient, yet flexible and reusable DNN acceleration platform, we present *OpenGeMM*, an open-source<sup>1</sup> and programmable GeMM acceleration platform with high flexibility and efficiency for edge AI. *OpenGeMM*'s overall system architecture is presented in Figure 1. Specifically,

- We propose a highly parameterized Chisel-coded GeMM accelerator hardware generator with 3D spatial unrollings, offering ease of customization and efficient data reuse (Section 2).
- We provide an efficient system integration platform with a lightweight RISC-V host processor and a tightly coupled memory subsystem, named *OpenGeMM*. For maximizing system utilization, three mechanisms are introduced, namely configuration pre-loading, input pre-fetching with output buffering, and programmable strided memory access (Section 3).
- Experimental results show that *OpenGeMM* achieves sustained high utilization ranging from 81.89% to 99.34% across diverse DNN workloads. Besides,  $3.58\times$  to  $16.40\times$  normalized throughput speedup is derived compared to open-source state-of-the-art (SotA) accelerator solutions stemmed from *OpenGeMM*'s high system utilization. Moreover, *OpenGeMM* shows 4.68 TOPS/W system power efficiency and the best operation-area efficiency among peer solutions (Section 4).

## 2 EFFICIENCY AND VERSATILITY IN GEMM ACCELERATOR GENERATION

We start by diving into the GeMM accelerator hardware generator, which aims for efficiency across a wide variety of workloads, through a combination of design time configurability and run-time programmability, to always ensure maximal spatial and temporal data reuse.

### 2.1 GeMM Accelerator Dataflow

The dataflow of the GeMM accelerator is depicted in Figure 2. The accelerator targets GeMM operations of dimension  $(M, K, N)$  as shown in Equation 1:

$$C_{M,N} = A_{M,K} \times B_{K,N} \quad (1)$$

<sup>1</sup>*OpenGeMM* is available open-source at [https://github.com/KULeuven-MICAS/snax\\_cluster](https://github.com/KULeuven-MICAS/snax_cluster).

The computation process involves splitting large matrices into tiles which can be executed in one cycle on the GeMM accelerator. Within *OpenGeMM*, this process is represented as 6 nested loops, which can be further categorized into spatial unrollings and temporal unrollings. Spatial unrollings (the 3 inner-most loops in Figure 2) represent spatial computation parallelism within a single clock cycle. Temporal unrollings (the 3 outer-most loops in Figure 2) reflect the sequential processing order of different tiles, while optimal unrollings will target to maximize local data reuse and minimize the stalls through proper loop ordering.

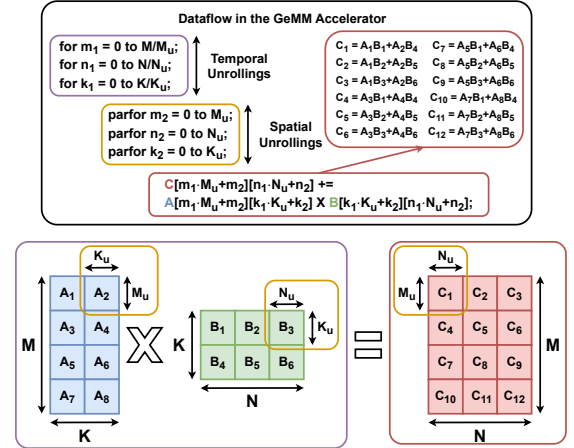
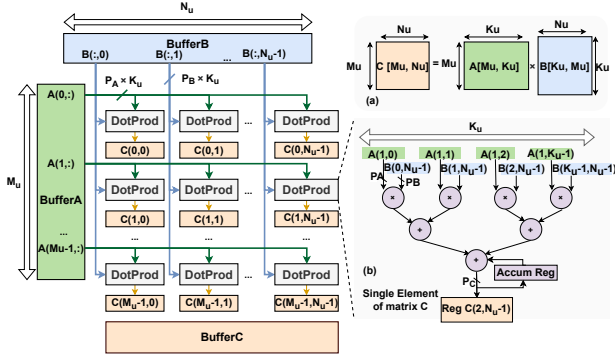


Figure 2: Dataflow representation in the GeMM accelerator hardware generator.

### 2.2 Exploiting 3D Spatial Unrollings to Maximize Spatial Data Reuse

GeMM accelerator spatially process a tile matrix  $A'$  of size  $(M_u, K_u)$  and a tile matrix  $B'$  of size  $(K_u, N_u)$  to produce a tile matrix  $C'$  of size  $(M_u, N_u)$ , as shown in Figure 3(a). To maximize spatial data reuse, it is important to reuse every fetched data element of  $A'$  and  $B'$  as much as possible. To ensure this, the GeMM array datapath is conceptualized as a 3D MAC (Multiply-Accumulate) array, as depicted in Figure 3. The 3D MAC array is organized as a  $(M_u, N_u)$ -sized mesh of  $K_u$ -sized vector dot product units (*DotProd* as detailed in Figure 3(b)) to spatially unroll all dimensions of matrices  $A'$ ,  $B'$ , and  $C'$ . The 3D MAC array is adapted to match with the 3 nested spatial unrollings for GeMM processing. Specifically, vectors from  $A'$  matrix and vectors from  $B'$  matrix are broadcasted horizontally and vertically among the *DotProd* array, maximizing spatial data reuse. Within one *DotProd*,  $K_u$  multiplication results are combinatorially accumulated to get one result of  $C'$ .

*OpenGeMM* supports design-time configurations of the *DotProd* array size and the size of each *DotProd* unit. This feature enables a flexible generation of a wide range of accelerators, such as dot-product units, outer-dot product units, vector-matrix multiplication accelerators, or matrix-matrix multiplication accelerators. Therefore, varied optimized spatial unrollings can be implemented based on these  $(M_u, K_u, N_u)$  parameters to accommodate the diverse computational requirements issued from different applications.



**Figure 3: GeMM accelerator hardware generator microarchitecture. (a) Matrix multiplication that GeMM accelerator processes in one cycle with 3D spatial unrollings. (b) DotProd microarchitecture.**

### 2.3 Exploiting Temporal Data Reuse to Minimize Memory Access

Temporal unrollings should be properly ordered to maximize the local data reuse and avoid unnecessary memory conflicts. Depending on whether the innermost temporal loop is weight-relevant or output-relevant, the dataflow can typically be categorized into weight-stationary and output-stationary. While weight-stationary keeps weight unchanged, output stationary dataflow fits better with GeMM operation, which can be verified through existing DNN dataflow design space exploration (DSE) frameworks [20]. The underlying rationale is the precision of the partial sum is often larger than the weight, leading to higher cost when the partial sum is to be updated every cycle. Take a typical convolutional layer with input tensor size of  $(O_x, O_y, C)$  and kernel size of  $(K, F_x, F_y, C)$  as an example, after im2col [21], the convolution operation is translated to matrix multiplication with matrix A of the size of  $(O_x \cdot O_y, F_x \cdot F_y \cdot C)$  and matrix B of the size of  $(F_x \cdot F_y \cdot C, K)$ . Since  $F_x \cdot F_y \cdot C$  is typically much larger than  $O_x \cdot O_y$ , reusing the partial sum in  $F_x \cdot F_y \cdot C$  dimension temporally saves more data bandwidth and energy. With this observation, *OpenGeMM* implements an output stationary dataflow supported by an output accumulation register inside each DotProd unit, with the innermost temporal loop iterating from  $k1 = 0$  to  $K/K_u$ .

All these 6 nested loop processes are handled through a built-in hardware loop controller within the GeMM accelerator, which is in charge of the timely input data request, outputting of result data, and accumulator resets. GeMM accelerator can be programmed at run-time with maximum hardware loop upper bound when the required data amount reaches the on-chip buffer capacity. For even larger matrices, the GeMM accelerator can be called multiple times through software controllers, eg., RISC-V core, to handle extra tiling as more nested temporal loops on higher-level memories.

## 3 SYSTEM ARCHITECTURE FOR HIGH UTILIZATION AND PROGRAMMABILITY

### 3.1 OpenGeMM System Architecture

To guarantee the GeMM accelerator can be smoothly integrated with standard SoCs, we propose the *OpenGeMM* platform (Figure 1)

to enhance programmability and maximize GeMM core throughput. It incorporates the GeMM accelerator mentioned earlier, as well as a compact RV32I host core, a tightly coupled multi-bank scratchpad memory, and three data streamers for efficient memory access. *OpenGeMM* offers extensive customization capabilities, with design time parameters summarized in Table 1.

**Table 1: Customizable *OpenGeMM* design-time parameters and case study configuration.**

Parameters	Meaning	Case study values
<b>Parameters for GeMM core</b>		
$M_u$	Number of rows of the array	8
$N_u$	Number of columns of the array	8
$K_u$	Size of each DotProd	8
$P_A$	Integer bit precision of A	8
$P_B$	Integer bit precision of B	8
$P_C$	Integer bit precision of C	32
<b>Parameters for memory system</b>		
$D_{stream}$	Pre-fetch buffer and output buffer depth	3
$R_{mem}$	Input memory ports	16
$W_{mem}$	Output memory ports	32
$P_{word}$	Memory port data width	64
$N_{bank}$	Number of banks	32
$D_{mem}$	Bank depth	1056

Specifically, *OpenGeMM* utilizes a lightweight 32-bit integer RISC-V Snitch core [22] for programming the GeMM compute core using standard RISC-V Configuration and Status Registers (CSR) instructions [23], while minimizing control area overhead. A specific register address range is allocated for the accelerator CSR configurations. A dedicated CSRManager module facilitates communication between the Snitch core and GeMM core through CSR operations, achieving high configuration bandwidth (32 bits/cycle). Multiple accelerator configurations can be consolidated into a single CSR to optimize configuration cycles. Since the CSR instruction is already part of the RISC-V ISA, there is no need to modify the RISC-V control core and the compiler, greatly alleviating the accelerator system integration and programming challenge.

To ensure efficient memory access, we tightly couple a wide-bandwidth, software-controlled multi-banked scratchpad memory (SPM) to the GeMM core. The multi-banked SPM supports configurable number of read ( $R_{mem}$ ) and write ( $W_{mem}$ ) ports with data width ( $P_{word}$ ), organized into multiple banks ( $N_{bank}$ ). Additionally, data streamers between the multi-banked SPM and GeMM core employ programmable hardware loops for efficient and autonomous data access catering to the GeMM core in a streaming way.

To improve the utilization problem in existing works, three system-level mechanisms are further introduced within *OpenGeMM*, which are detailed in subsequent subsections.

### 3.2 Configuration Pre-loading

Due to the sequential programming of numerous CSRs, including hardware loop bounds related to workload size  $(M, K, N)$ , base addresses and strides related to memory access, the programming

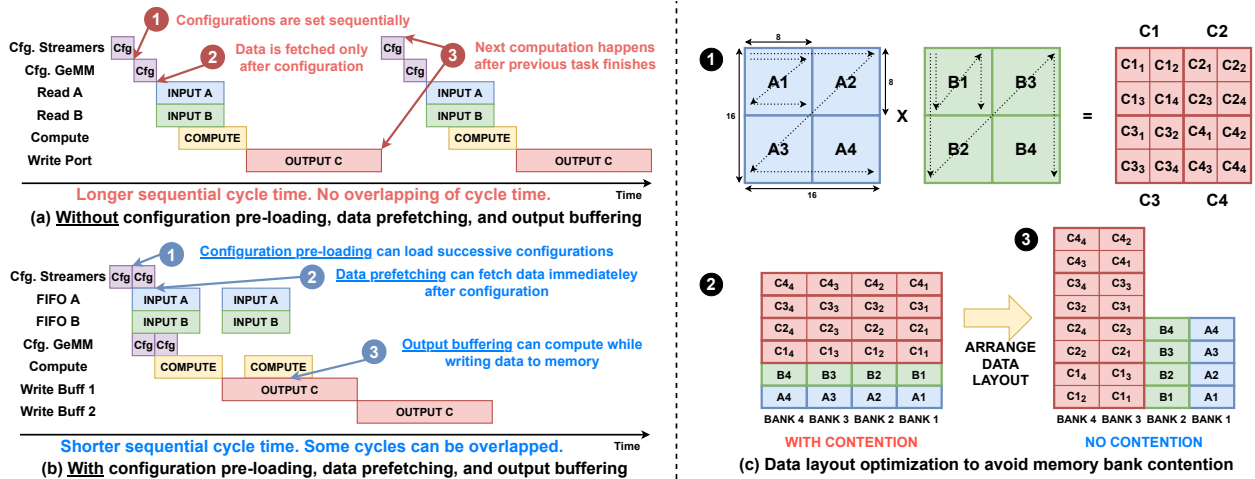


Figure 4: (a) Scenario without configuration pre-loading, input pre-fetch, and output buffering. (b) Conceptual visualizations for configuration pre-loading, input pre-fetch, and output buffering. (c) Data layout optimization example.

cycle can be lengthy, as shown in Figure 4(a) ❶. To hide the configuration time, we introduce a configuration pre-loading (CPL) mechanism. It allows the host to pre-load the GeMM core configuration for the next computation, while the current computation is being executed, effectively overlapping configuration time with computation time, as depicted in Figure 4(b) ❶.

### 3.3 Input Pre-fetch and Output Data Buffering

To minimize computation stalls, we incorporate a data buffer within the data streamer to allow continuous pre-fetching of data until the buffer reaches its capacity. As long as there is space in the buffer (data being consumed by the GeMM core), it will actively pre-fetch data. This dynamic producer-consumer mechanism aims to maintain high utilization of the GeMM array. The buffer depth is a configurable parameter set at design time, based on the amount of data that would like to be pre-fetched. Figure 4(b) ❷ illustrates that immediately after configuring the streamer, the data buffers begin pre-fetching data while the GeMM core is being configured.

The output stationary nature ensures that the GeMM core writes back a result every  $K/K_u$  computational cycles, facilitating the reduction of output memory stalls through an output buffering mechanism. Specifically, a configurable number of output data buffers alternate between storing the output from the GeMM core and writing the output matrix to memory in a round-robin fashion. Figure 4(b) ❸ illustrates the timing utilization of the write ports. This allows computation to proceed concurrently with writing the output of the last result. Without the input pre-fetch and output data buffering, the GeMM core utilization can be lower because of idle cycles caused by input and output memory stalls, as shown in Figure 4(a) ❷ and ❸.

### 3.4 Strided Memory Access

The compiler can exploit strided data access [24] to optimize the data layout by interleaving access, thereby minimizing bank conflicts and maximizing the utilization of the GeMM core. Figure 4(c) illustrates an example of data layout optimization. Figure 4(c) ❶ shows a set of matrices and their sub-matrices for GeMM operation input. These matrices can be organized contiguously in either row-major or column-major order in memory as depicted

in Figure 4(c) ❷. This layout will lead to bank contentions because sub-matrices A1 and B1 are accessed in the same bank. However, by transforming the data layout as shown in Figure 4(c) ❸, bank contentions can be avoided.

To address this, we equip each data streamer with a configurable strided address generation [24] unit (AGU) to support flexible data access to relieve the memory bank contentions. Specifically,

- *At design time*, we configure the AGU such that it matches the GeMM core’s port width and the address generation pattern, such as how many nested loops are needed for strided address generation, of operands  $A$ ,  $B$ , and  $C$ . These are also related to the number of multi-banked SPM read ports  $R_{mem}$ , write ports  $W_{mem}$ , and their width  $P_{word}$ .
- *At run time*, we program the hardware loop bounds, base addresses, and two-dimensional memory strides for each data streamer to generate the corresponding data layout address.

## 4 OPENGEMM EVALUATION AND SOTA COMPARISON

### 4.1 Evaluation Setup

We evaluate the proposed *OpenGeMM* system at the register transfer level (RTL), utilizing Chisel [25] for designing the GeMM accelerator hardware generator and SystemVerilog to implement all other platform components built upon [22]. We generate one *OpenGeMM* instance using the case study parameters listed in Table 1. We choose an 8x8x8 GeMM array to achieve a good balance between spatial utilization and hardware throughput for typical GeMM workloads. For performance and utilization evaluation, we conduct cycle-accurate RTL simulation using Verilator. The system is then synthesized with Synopsys Design Compiler under the TSMC 16nm FFC process technology at a clock frequency of 200MHz and a supply voltage of 0.675V. Power analysis is conducted using Synopsys PrimeTime.

### 4.2 Utilization Analysis

An ablation experiment is performed to assess the effectiveness of the proposed three mechanisms in enhancing the GeMM core’s utilization. We conduct experiments on the 8x8x8 GeMM accelerator with 500 different computational matrix sizes  $(M, K, N)$ , randomly

choosing from  $M, K, N \in \{8, 16, 24, \dots, 256\}$ . To access the benefits of proposed mechanisms, the combinations consisting of different techniques are enabled to evaluate their individual impact on utilization. Each workload is repeated 10 times to observe the effect of the configuration pre-loading mechanism.

Figure 5 hence presents the utilization results in a box-plot format. Specifically, incorporating the configuration pre-loading (CPL) (Arch②) results in a median utilization improvement of 1.4 $\times$  compared with baseline (Arch①). When combining input pre-fetching and output buffering (Buf.Depth=2) (Arch③), the median utilization improves by an additional 2.02 $\times$  compared with Arch②, demonstrating the effectiveness of the input data pre-fetching and output data buffering. Additionally, employing strided memory access (SMA) (Arch④) increases median utilization by 1.18 $\times$  compared with Arch③, showing the data layout optimization effect. Overall, implementing all three techniques (Arch④) enhances median utilization by 2.78 $\times$  compared to the baseline *OpenGeMM* platform (Arch①). Exploring the impact of increasing buffer depth to 3 and 4 shows a consistent increase in utilization with less variation across different matrix sizes.

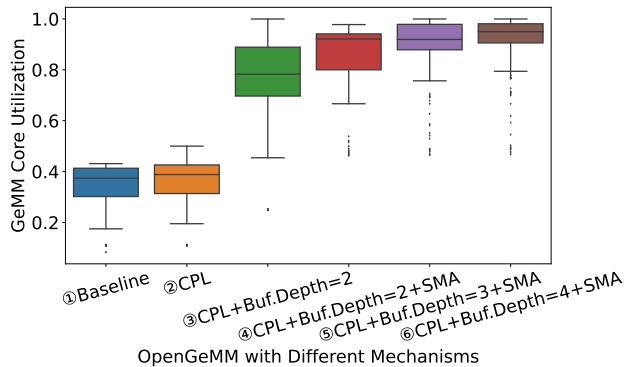


Figure 5: Utilization analysis of *OpenGeMM* under 500 random computational matrix sizes and different utilization enhancement techniques.

Table 2: Utilization (in %) and performance (in cycles) of *OpenGeMM* on real DNN workloads.

	MobileNetV2	ResNet18	ViT-B-16	BERT-Base
SU*	87.36	96.01	98.41	99.54
TU <sup>†</sup>	93.74	99.72	99.75	99.80
OU <sup>‡</sup>	81.89	95.74	98.16	99.34
CC <sup>§</sup>	$3.33 \times 10^8$	$9.29 \times 10^8$	$1.79 \times 10^{10}$	$4.93 \times 10^{10}$

[\*] Spatial utilization.  
[‡] Overall utilization.

[<sup>†</sup>] Temporal utilization.  
[§] Cycle count.

### 4.3 Real DNNs Benchmarking

To evaluate the performance of *OpenGeMM* in practical scenarios, several typical CNN and Transformer workloads, including ResNet18 [28], MobileNetV2 [29], Vision Transformer [30] and Bert-Base [31] are benchmarked. Our focus is specifically on the energy- and latency-dominant blocks, including convolutional layers (executed via im2col [21]), multi-head attention, multilayer perceptron layers, and fully connected layers within these models.

The utilization and performance<sup>2</sup> results of these models are presented in Table 2. Due to the irregular matrix sizes inherent in these workloads, *OpenGeMM* does not achieve full spatial utilization. For example, in the MobileNetV2 model that has rich depth-wise convolutions, the spatial utilization is only 87.36%, indicating that the im2col-ed matrix sizes are not multiples of  $(M_u, K_u, N_u)$ . Moreover, the depth-wise convolutions have fewer channels (tick channels), resulting in smaller K values and slightly lower temporal utilization compared to other workloads. Conversely, in ResNet18 where channel sizes are larger, temporal utilization is as high as 95.74%. In Transformer workloads with regular matrix sizes and no small K values, *OpenGeMM* consistently achieves near 100% spatial and temporal utilization, approaching peak performance. Despite varying computation characteristics across different workloads, the overall utilization of the GeMM core remains consistently high, ranging from 81.89% to 99.34%. This indicates efficient execution of diverse DNN workloads on the run-time programmable *OpenGeMM* platform.

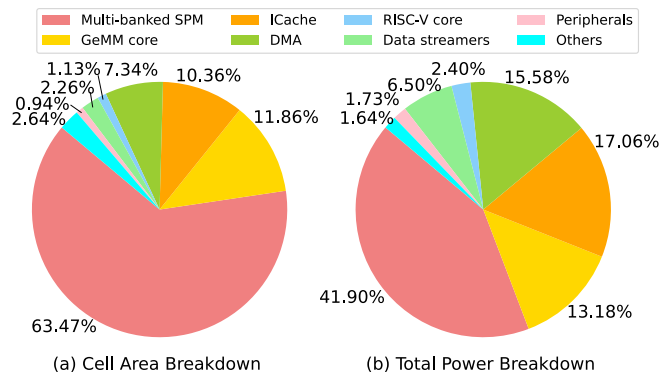


Figure 6: *OpenGeMM* cell area and total power breakdown.

### 4.4 Area and Power Evaluation

The workload for system power estimation involves block matrix multiplication with a size of  $(32, 32, 32)$ . *OpenGeMM* system occupies a cell area of  $0.531 \text{ mm}^2$  and consumes a total system power of 43.8 mW when operating at 200MHz. Achieving a peak performance of 204.8 GOPS, the *OpenGeMM* demonstrates a system efficiency of 4.68 TOPS/W.

The detailed area and power breakdown of the *OpenGeMM* system is illustrated in Figure 6, with all other system components encompassed, such as the instruction cache and DMA. The largest area component is the 270KiB multi-banked SPM including the interconnect towards the streamers, occupying 63.47% of the total area breakdown, followed by the GeMM core at 11.86%. In terms of power breakdown, multi-banked SPM accounts for 41.90%, instruction cache for 17.06%, and GeMM core for 13.18%. Data streamers for data movement occupy 2.26% of total area and 6.5% of total system power. It is important to note that the RISC-V control overhead is negligible, around 1.13% of the entire system cost and 2.4% of system power, offering *OpenGeMM* efficiency with minimal hardware overheads.

<sup>2</sup>The data movement cycles between the off-chip DRAM and the on-chip SRAM are not counted.

Table 3: State-of-the-Art Comparison. The efficiency metrics shown for each platform are system efficiencies.

Accelerator	SIGMA [26]	CONNA [13]	Gemmini [12]	DIANA [19]	RBE [11]	RedMule [15]	OpenGeMM This Work
Tech (nm)	28	65	22	22	22	22	16
Area (mm <sup>2</sup> )	65	2.36	1.03	8.91	2.42	0.73	0.62 <sup>†</sup>
Memory (KiB)	6,000	144	256	512	128	128	270
Freq (MHz)	500	200	1000	280	420	470	200
Peak Perf. (GOPS)	16,000	102.4	512	224 (Dig.) 40 (AIMC)	637 (2b) 91 (8b)	89	204(8b)
Peak Eff. (TOPS/W)	0.48	0.856	-	1.7 (Dig.) 4 (AIMC)	12.4 (2b) 0.74 (8b)	1.6	4.68(8b)
Peak Perf./Area (GOPS/mm <sup>2</sup> )	246	43	497	25 (Dig.) 4.5 (AIMC)	263 (2b) 37 (8b)	121	329(8b) <sup>†</sup>
Op-Area-Eff. (TOPS/W/mm <sup>2</sup> )	0.0073	0.363	-	0.2 (Dig.) 0.44 (AIMC)	5.12 (2b) 0.31 (8b)	2.2	7.55(8b) <sup>†</sup>
Supported Precision	BFP 16, FP 32	INT 4, 8, 16, 32	INT8	INT 8	INT 2, 4, 8	FP 8, 16	INT 2, 4, 8 <sup>§</sup>
Open Source	✓	×	✓	✓	✓	✓	✓
Generated Arch.*	×	✓	✓	×	×	×	✓
Design- and Run- time Config. <sup>¶</sup>	×	✓	✓	×	✓	✓	✓

\* Means the design comes from a hardware generator like Chisel.

<sup>¶</sup> Has parameters configurable during design-time (or hardware design configurations) and run-time (or programmable).

<sup>†</sup> After placement and routing layout area estimation with 60% cell density according to [27].

<sup>§</sup> Design-time configurable.

#### 4.5 State of The Art Comparison

We now compare *OpenGeMM* against the state-of-the-art (SotA) of flexible DNN acceleration systems, as summarized in Table 3. Specifically, we benchmark the throughput of *OpenGeMM* against the SotA GeMM accelerator generation system Gemmini [12], utilizing performance data from [32].

Figure 7 illustrates the area-normalized throughput comparison (in  $\text{GOPS}/\text{mm}^2$ ) among the Gemmini in output-stationary (OS) mode and weight-stationary (WS) mode, and *OpenGeMM* across matrix sizes ranging from (8, 8, 8) to (128, 128, 128). Compared to Gemmini OS and WS, *OpenGeMM* exhibits normalized throughput speedups ranging from 3.75 $\times$  to 16.40 $\times$  and 3.58 $\times$  to 15.66 $\times$ , respectively. The exceptional performance of *OpenGeMM* is attributed to the high utilization of the GeMM core, approaching ideal peak performance for these workloads. In contrast, Gemmini falls short of maintaining high temporal utilization (on average 6.25%) on these workloads, because of intensive memory stalls, resulting in lower actual throughput.

In summary, *OpenGeMM*'s lightweight RISC-V core and tight memory coupling reduce hardware overhead from control and data access while the GeMM core architecture maximizes spatial and temporal data reuse. Moreover, *OpenGeMM* introduces three mechanisms to achieve sustained high utilization. This results in *OpenGeMM* achieving high system energy efficiency and the best operation-area efficiency across all SotAs with int8 data precision. These features make *OpenGeMM* suitable for efficient edge DNN computing.

## 5 CONCLUSION

This paper introduces *OpenGeMM*, an open-source GeMM acceleration platform targeting edge AI applications. *OpenGeMM* is built around a Chisel-based GeMM accelerator, associated with a lightweight RISC-V processor and a tightly coupled memory system. To improve the hardware utilization and therefore the processing

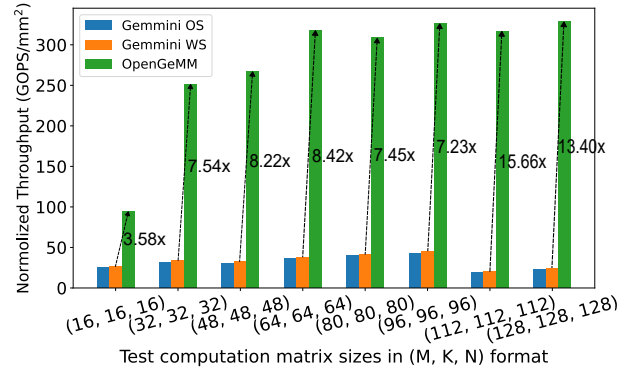


Figure 7: Comparison of normalized throughput ( $\text{GOPS}/\text{mm}^2$ ) for Gemmini [12] in output stationary (OS) mode, Gemmini [12] in weight stationary (WS) mode, and *OpenGeMM* across various computational matrix sizes.

efficiency, three mechanisms are introduced at the system level. The experiments demonstrate that these mechanisms can improve the MAC array utilization of *OpenGeMM* consistently up to 81.89%-99.34% across various DNN workloads. Compared with the SotA, *OpenGeMM* shows 4.68 TOPS/W system power efficiency and 3.58 $\times$  to 16.40 $\times$  normalized throughput speedup.

## ACKNOWLEDGMENT

This project has been partly funded by the European Research Council (ERC) under grant agreement No. 101088865, the European Union's Horizon 2020 program (CONVOLVE) under grant agreement No. 101070374, the Flanders AI Research Program, Research Foundation-Flanders (FWO) under grant 1SE7723N, and KU Leuven. Guilherme Paim expresses gratitude to the CAPES Brazilian Foundation for their financial support in past grants and for accepting the novation agreement that allowed him to work abroad.

## REFERENCES

- [1] Nikolaos Schizas, Aristeidis Karras, Christos Karras, and Spyros Sioutas. Tinyml for ultra-low power ai and large scale iot deployments: A systematic review. *Future Internet*, 14(12):363, 2022.
- [2] Cristina Silvano, Daniele Ielmini, Fabrizio Ferrandi, Leandro Fiorin, Serena Curzel, Luca Benini, Francesco Conti, Angelo Garofalo, Cristian Zambelli, Enrico Calore, Sebastiano Fabio Schifano, Maurizio Palesi, Giuseppe Ascia, Davide Patti, Stefania Perri, Nicola Petra, Davide De Caro, Luciano Lavagno, Teodoro Urso, Valeria Cardellini, Gian Carlo Cardarilli, and Robert Birke. A survey on deep learning hardware accelerators for heterogeneous hpc platforms, 2023.
- [3] Yiran Chen, Yuan Xie, Linghao Song, Fan Chen, and Tianqi Tang. A survey of accelerator architectures for deep neural networks. *Engineering*, 6(3):264–274, 2020.
- [4] Trio Adiono, Rhessa Muhammad Ramadhan, Nana Sutisna, Infall Syafalni, Rahmat Mulyawan, and Chang-Hong Lin. Fast and scalable multicore yolov3-tiny accelerator using input stationary systolic architecture. *IEEE Transactions on Very Large Scale Integration (VLSI) Systems*, 2023.
- [5] Koen Goetschalckx and Marian Verhelst. Depfin: A 12nm, 3.8 tops depth-first cnn processor for high res. image processing. In *2021 Symposium on VLSI Circuits*, pages 1–2. IEEE, 2021.
- [6] Tae Jun Ham, Sung Jun Jung, Seonghak Kim, Young H Oh, Yeonhong Park, Yoonho Song, Jung-Hun Park, Sanghee Lee, Kyoung Park, Jae W Lee, et al. A<sup>3</sup>: Accelerating attention mechanisms in neural networks with approximation. In *2020 IEEE International Symposium on High Performance Computer Architecture (HPCA)*, pages 328–341. IEEE, 2020.
- [7] Frans Sijstermans. The nvidia deep learning accelerator. In *Hot Chips*, volume 30, pages 19–21, 2018.
- [8] Shangong Feng, Junning Wu, Shengang Zhou, and Renwei Li. The implementation of lenet-5 with nvdla on risc-v soc. In *2019 IEEE 10th International Conference on Software Engineering and Service Science (ICSESS)*, pages 39–42. IEEE, 2019.
- [9] Abraham Gonzalez and Charles Hong. A chipyard comparison of nvdla and gemmini. *Berkeley, CA, USA, Tech. Rep. EE*, pages 290–2, 2020.
- [10] Andrew Waterman, Yunsup Lee, David A Patterson, and Krste Asanović. The risc-v compressed instruction set manual, version 1.7. *EECS Department, University of California, Berkeley, UCB/EECS-2015-157*, 2015.
- [11] Francesco Conti, Gianna Paulin, Angelo Garofalo, Davide Rossi, Alfio Di Mauro, Georg Rutishauser, Gianmarco Ottavi, Manuel Eggiman, Hayate Okuhara, and Luca Benini. Marsellus: A heterogeneous risc-v ai-iot end-node soc with 2–8 b dnn acceleration and 30 *IEEE Journal of Solid-State Circuits*, 59(1):128–142, January 2024. ISSN 1558-173X. doi: 10.1109/jssc.2023.3318301. URL <http://dx.doi.org/10.1109/JSSC.2023.3318301>.
- [12] Hasan Genc, Seah Kim, Alon Amid, Ameer Haj-Ali, Vighnesh Iyer, Pranav Prakash, Jerry Zhao, Daniel Grubb, Harrison Liew, Howard Mao, et al. Gemmini: Enabling systematic deep-learning architecture evaluation via full-stack integration. In *2021 58th ACM/IEEE Design Automation Conference (DAC)*, pages 769–774. IEEE, 2021.
- [13] Sang-Soo Park and Ki-Seok Chung. Conna: Configurable matrix multiplication engine for neural network acceleration. *Electronics*, 11(15), 2022. ISSN 2079-9292. doi: 10.3390/electronics11152373. URL <https://www.mdpi.com/2079-9292/11/15/2373>.
- [14] Francesco Conti, Pasquale Davide Schiavone, and Luca Benini. Xnor neural engine: A hardware accelerator ip for 21.6-fj/op binary neural network inference. *IEEE Transactions on Computer-Aided Design of Integrated Circuits and Systems*, 37(11):2940–2951, November 2018. ISSN 1937-4151. doi: 10.1109/tcad.2018.2857019. URL <http://dx.doi.org/10.1109/TCAD.2018.2857019>.
- [15] Yvan Tortorella, Luca Bertaccini, Luca Benini, Davide Rossi, and Francesco Conti. Redmule: A mixed-precision matrix-matrix operation engine for flexible and energy-efficient on-chip linear algebra and tinyml training acceleration. *arXiv preprint arXiv:2301.03904*, 2023.
- [16] Süleyman Savas, Zain Ul-Abdin, and Tomas Nordström. Designing domain-specific heterogeneous architectures from dataflow programs. *Computers*, 7(2): 27, 2018.
- [17] Man Shi, Steven Coleman, Charlotte VanDeMieroop, Antony Joseph, Maurice Meijer, Wim Dehaene, and Marian Verhelst. Ccmds: Cross-layer dataflow optimization for dnn accelerators exploiting multi-bank memories. In *2023 24th International Symposium on Quality Electronic Design (ISQED)*, pages 1–8, 2023. doi: 10.1109/ISQED57927.2023.10129330.
- [18] Xiaoling Yi, Jiangnan Yu, Zheng Wu, Xiankui Xiong, Dong Xu, Chixiao Chen, Jun Tao, and Fan Yang. Nnasim: An efficient event-driven simulator for dnn accelerators with accurate timing and area models. In *2022 IEEE International Symposium on Circuits and Systems (ISCAS)*, pages 2806–2810. IEEE, 2022.
- [19] Pouya Houshmand, Giuseppe M. Sarda, Vikram Jain, Kodai Ueyoshi, Ioannis A. Papistas, Man Shi, Qilin Zheng, Debjyoti Bhattacharjee, Arindam Mallik, Peter Debacker, Diederik Verkest, and Marian Verhelst. Diana: An end-to-end hybrid digital and analog neural network soc for the edge. *IEEE Journal of Solid-State Circuits*, 58(1):203–215, 2023. doi: 10.1109/JSSC.2022.3214064.
- [20] Linyan Mei, Pouya Houshmand, Vikram Jain, Sebastian Giraldo, and Marian Verhelst. Zigzag: Enlarging joint architecture-mapping design space exploration for dnn accelerators. *IEEE Transactions on Computers*, 70(8):1160–1174, 2021.
- [21] Andrew Anderson, Aravind Vasudevan, Cormac Keane, and David Gregg. Low-memory gemm-based convolution algorithms for deep neural networks. *arXiv preprint arXiv:1709.03395*, 2017.
- [22] Florian Zaruba, Fabian Schuiki, Torsten Hoefler, and Luca Benini. Snitch: A tiny pseudo dual-issue processor for area and energy efficient execution of floating-point intensive workloads. *IEEE Transactions on Computers*, 70(11):1845–1860, 2020.
- [23] Andrew Waterman, Krste Asanović, and John Hauser. *The RISC-V Instruction Set Manual, Volume II: Privileged Architecture*. RISC-V International, December 2021. Document Version 20211203.
- [24] Fabian Schuiki, Florian Zaruba, Torsten Hoefler, and Luca Benini. Stream semantic registers: A lightweight risc-v isa extension achieving full compute utilization in single-issue cores. *IEEE Transactions on Computers*, 70(2):212–227, 2020.
- [25] Jonathan Bachrach, Huy Vo, Brian Richards, Yunsup Lee, Andrew Waterman, Rimas Avizienis, John Wawrzynek, and Krste Asanović. Chisel: constructing hardware in a scala embedded language. In *Proceedings of the 49th Annual Design Automation Conference*, pages 1216–1225, 2012.
- [26] Eric Qin, Ananda Samajdar, Hyoukjun Kwon, Vineet Nadella, Sudarshan Srinivasan, Dipankar Das, Bharat Kaul, and Tushar Krishna. Sigma: A sparse and irregular gemm accelerator with flexible interconnects for dnn training. In *2020 IEEE International Symposium on High Performance Computer Architecture (HPCA)*, pages 58–70, 2020. doi: 10.1109/HPCA47549.2020.00015.
- [27] Gianna Paulin, Matheus Cavalcante, Paul Scheffler, Luca Bertaccini, Yichao Zhang, Frank Gürkaynak, and Luca Benini. Soft tiles: Capturing physical implementation flexibility for tightly-coupled parallel processing clusters. In *2022 IEEE Computer Society Annual Symposium on VLSI (ISVLSI)*, pages 44–49. IEEE, 2022.
- [28] Kaiming He, Xiangyu Zhang, Shaoqing Ren, and Jian Sun. Identity mappings in deep residual networks. In *Computer Vision—ECCV 2016: 14th European Conference, Amsterdam, The Netherlands, October 11–14, 2016, Proceedings, Part IV 14*, pages 630–645. Springer, 2016.
- [29] Mark Sandler, Andrew Howard, Menglong Zhu, Andrey Zhmoginov, and Liang-Chieh Chen. Mobilenetv2: Inverted residuals and linear bottlenecks. In *Proceedings of the IEEE conference on computer vision and pattern recognition*, pages 4510–4520, 2018.
- [30] Alexey Dosovitskiy, Lucas Beyer, Alexander Kolesnikov, Dirk Weissenborn, Xiuhua Zhai, Thomas Unterthiner, Mostafa Dehghani, Matthias Minderer, Georg Heigold, Sylvain Gelly, et al. An image is worth 16x16 words: Transformers for image recognition at scale. *arXiv preprint arXiv:2010.11929*, 2020.
- [31] Jacob Devlin, Ming-Wei Chang, Kenton Lee, and Kristina Toutanova. Bert: Pre-training of deep bidirectional transformers for language understanding. *arXiv preprint arXiv:1810.04805*, 2018.
- [32] Abraham Gonzalez, Jerry Zhao, Ben Korpan, Hasan Genc, Colin Schmidt, John Wright, Ayan Biswas, Alon Amid, Farhana Sheikh, Anton Sorokin, et al. A 16nm 2 106.1 gops/w heterogeneous risc-v multi-core multi-accelerator soc in low-power 22nm finfet. In *ESSCIRC 2021-IEEE 47th European Solid State Circuits Conference (ESSCIRC)*, pages 259–262. IEEE, 2021.